Refereed Proceedings

The 13th International Conference on Fluidization - New Paradigm in Fluidization Engineering

Engineering Conferences International *Year* 2010

CFD-DEM SIMULATION OF SYNGAS-TO-METHANE PROCESS IN A FLUIDIZED-BED REACTOR

Changning Wu, Dayong Tian* Yi Cheng†

*Tsinghua University

†Tsinghua University, yicheng@tsinghua.edu.cn

CFD-DEM SIMULATION OF SYNGAS-TO-METHANE PROCESS IN A FLUIDIZED-BED REACTOR

Changning Wu, Dayong Tian and Yi Cheng *
Department of Chemical Engineering, Tsinghua University, Beijing 100084, China
* Corresponding author. Fax: 86-10-62772051; E: yicheng@tsinghua.edu.cn

ABSTRACT

The CFD-DEM coupled approach was used to simulate the gas-solid reacting flows in a lab-scale fluidized-bed reactor for syngas-to-methane (STM) process. The simulation results captured the major features of the reactor performance including unwanted defluidization. The fluidized-bed reactor showed good performances, such as in preventing the catalyst particles from overheating and sintering.

Keywords: syngas; methanation; fluidized bed; defluidization; CFD-DEM; reacting flow simulation

INTRODUCTION

The production of substitute natural gas (SNG) from coal provides an alternative fuel due to limited petroleum and natural gas (1,2). The syngas-to-methane (STM) process converts the syngas produced from the coal gasifiers to SNG (primarily methane) through the well-known methanation reactions, with a high exothermicity and a large decrease of gas volume in nature (2,3,4). Generally, the methanation reactions take place around 300~500 °C over supported noble metal catalysts in a methanation reactor. The temperature in the reactor should be controlled to prevent overheating of the catalyst particles due to the exothermic reaction. On the other hand, a high temperature is undesirable for methane formation from the viewpoint of thermodynamic equilibrium. Most of the methanation reactors have been reported as the type of fixed bed. In comparison with the fixed-bed reactor, the fluidized-bed reactor is better suited for the syngas-to-methane process because of its excellent heat removal capability (5). In principle, the fluidized-bed reactor should be superior to the fixed-bed reactor in the reactor performances, e.g., catalyst operating life (relative to the temperature profile of the catalyst particles) and ability to be scaled up. Oppositely, the decrease of fluidization quality in a fluidized-bed reactor due to the large decrease of gas volume should be well addressed.

The CFD-DEM modeling scheme, i.e., a computational fluid dynamics (CFD) model for gas-phase flow combined with a discrete element method (DEM) for particle movement, has been extended and applied to simulate the complex gas-solid reacting flows in fluidized-bed reactors for fluid catalytic cracking (FCC) process in our previous work (see Wu *et al*. (6)). In this study, the extended CFD-DEM modeling scheme was used to simulate the syngas-to-methane process accommodated in a fluidized-bed reactor. The model incorporates the descriptions for heat transfer behaviors between particles and between gas and particles, and the catalytic reaction kinetics for the STM process, together with the governing equations for the hydrodynamics. The distinct advantage of the present approach is that the particle temperature (i.e., reaction temperature) can be calculated in time accurately by tracking the history of the particle movement with the occurrence of heat transfer and chemical reactions.

MATHEMATICAL MODEL AND NUMERICAL SIMULATIONS

The CFD-DEM reacting flow model is mainly comprised of two parts. For gas phase, a set of conservation equations for the mass, momentum, energy and chemical species is integrated with the Realizable *k-ε* model. For particle phase, the three-equation linear dash-pot model (7,8) is employed to take full account of the particle-particle interactions at the micro-scale. The sub-model of heat transfer for particle phase mainly considers the thermal conduction between particles by using the thermal particle dynamics (TPD) approach proposed by Vargas and McCarthy (9). More details about the CFD-DEM reacting flow model could be found from Ref. (6).

The Inter-phase Coupling

The governing equations for the particle phase are coupled with those of the gas phase through the porosity and the inter-phase momentum, energy, *k* and *ε* source terms. In this study, the straightforward method given by Hoomans *et al.* (10) is used for the calculation of the porosity,

$$\varepsilon_{g,cell} = 1 - \frac{1}{V_{cell}} \sum_{\forall i \in cell} f_{cell}^{i} V_{p}^{i} \tag{1}$$

where f_{cell}^{i} is the fractional volume of particle *i* residing in the cell under consideration, V_p^i is the volume of particle *i*, and V_{cell} represents the volume of the computational cell. Hence, the backward mapping of a general variable φ_p on the Lagrangian particle position to a property on the Eulerian grid φ_{cell} can be done via

$$\varphi_{cell} = \sum_{\forall i \in cell} f_{cell}^{i} \varphi_{p} \tag{2}$$

A Kinetic Model to Describe the Syngas-To-Methane (STM) Process

The following five reactions, including methanation of CO, steam reforming of methane, and forward/reverse water gas shift reaction over a wide range of reaction temperature, are considered in the present kinetic model with the kinetic parameters achieved and validated at operating pressures of 5~30 atm (see Table 1).

$$CO + 3H_2 = CH_4 + H_2O, \qquad r_1 = A_1 \exp\left(-E_1/RT\right) p_{CO}^{a_1} p_{H_2}^{b_1} \tag{3}$$

$$CH_4 + H_2O = CO + 3H_2, \qquad r_2 = A_2 \exp\left(-E_2/RT\right) p_{CH_4}^{a_2} p_{H_2O}^{b_2} p_{CO}^{c_2} p_{H_2}^{d_2} \tag{4}$$

$$CH_4 + 2H_2O = CO_2 + 4H_2, \qquad r_3 = A_3 \exp\left(-E_3/RT\right) p_{CH_4}^{a_3} p_{H_2O}^{b_3} p_{CO_2}^{c_3} p_{H_2}^{d_3} \tag{5}$$

$$CO + H_2O = CO_2 + H_2, \qquad r_4 = A_4 \exp\left(-E_4/RT\right) p_{CO}^{a_4} p_{H_2O}^{b_4} \tag{6}$$

$$CO_2 + H_2 = CO + H_2O, \qquad r_5 = A_5 \exp\left(-E_5/RT\right) p_{CO_2}^{a_5} p_{H_2}^{b_5} \tag{7}$$

Table 1. Kinetic constants for the STM kinetic model (the catalyst: 14 wt% N_i/γ-Al_2O_3)

Reactions (r_i)	A_i (*)	E_i (J/mol)	a_i, b_i, c_i, d_i	ΔH_r^0 (J/mol)
i = 1	5.59E+05	9.16E+04	1.48, 1.50, 0, 0	-204723
i = 2	4.84E+04	1.17E+05	1.17, 0, 0.70, -1.32	204723
i = 3	3.35E+04	1.07E+05	1.28, 0, 1.18, -1.79	163521
i = 4	4.01E+01	5.00E+04	1.20, 0.10, 0, 0	-41203
i = 5	1.00E+09	2.00E+05	1.00, 0.50, 0, 0	41203

(*) the unit of frequency factor A_i is mol/kg_{cat}/s/atm^{ni}, where the index ni = a_i+b_i+c_i+d_i.

Table 2. Computation conditions and additional parameters

Particle Parameters	**Value**	**Operating conditions**	**Value**
diameter (m)	2.0e-4	Inlet gas temperature (K)	573~773
density (kg/m^3)	2225	gas mass flux (kg/m^2s)	0.134~2.01
heat capacity (J/kg/K)	1500	Inlet pressure (MPa)	1.8
thermal conductivity (W/m/K)	10.0	Wall temperature	= $T_{g,in}$
number of particles	~2,000	Wall heat transfer coef. (W/m^2K)	10.0
DEM model parameters	**p-p (p-w)**	Components of feed gases	wt%
normal spring constant (N/m)	140 (100)	CO	77.43
tangential spring constant (N/m)	140 (100)	H_2	18.69
rolling spring constant (N·m)	0.00005	CH_4	0
normal restitution coefficient	0.97	H_2O	0.22
tangential restitution coefficient	0.97	CO_2	0.27
rolling restitution coefficient	0.97	N_2	3.39
sliding friction coefficient	0.05	**Time step for simulation (s)**	
rolling friction coefficient (m)	0.00005	particle phase	5.0×10^{-6}
Notation: p = particle, w = wall		gas phase	5.0×10^{-5}

Numerical Method and Computational Conditions

The equations of gas flow were solved using a licensed FLUENT solver, while the DEM module and other sub-models were coded in C language as the user defined functions (UDFs) to connect with FLUENT. All the simulations of the gas-solid reacting flows were carried out in 2D domains either in fixed or in fluidized bed with the width of 8 mm and the height of 100 mm. The mesh for gas phase is 10 (W) × 200 (H). The computational conditions and the additional parameters are given in Table 2. The operating pressure in the reactors is 1.8 MPa, which is at the level of industrial operations for the syngas-to-methane process. The physical properties of each species are calculated by kinetic theory. The boundary conditions for gas phase are (1) the uniform mass flow inlet boundary condition, (2) the outflow boundary condition at the outlet, and (3) no slip, zero diffusive flux and convective heat transfer for the wall boundary condition. In the DEM model, the wall is treated as a fixed ball with a diameter large enough.

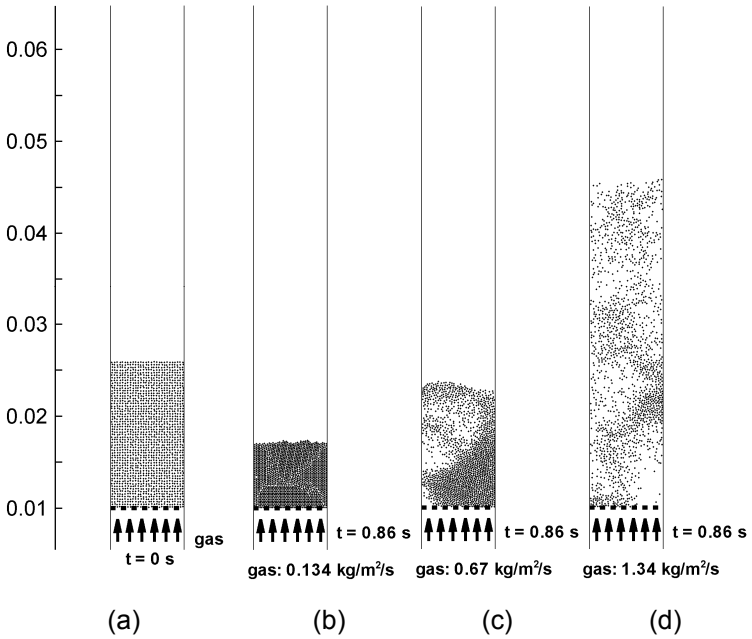

Figure 1. Transient spatial distributions of the particle phase at different gas mass fluxes ($T_{g,in}$ = 673 K, $\varepsilon_{p,0}$ = 0.261)

RESULTS AND DISCUSSION

Influence of Gas Feeding Rate

It is of great importance to control the fluidization quality in a fluidized-bed reactor for good syngas conversion and product selectivity. The transient spatial distributions of the particle phase at different gas mass fluxes are plotted in Fig. 1, with the same inlet gas temperature and catalyst particle inventory. The particles are distributed uniformly in the range of 0.01 ~ 0.03 m in height with an initial solids volume fraction ($\varepsilon_{p,0}$) of 0.261 (see Fig. 1a). At the gas mass flux (G_g) of 0.134 kg/m^2/s, although the superficial gas velocity (U_g) is 1.61 times of the minimum fluidization velocity (U_{mf}) estimated by assuming that the gas component is close to the one of the feed gases, almost all of the particles remain packed in the bottom region of the column after

enough time being blowed (see Fig. 1b and Table 3). This phenomenon is mainly caused by the fast methanation reaction involving a large decrease in the numbers of moles, that is, 4 to 2 as illustrated in Eq. (3) with a corresponding value of U_g/U_{mf} reduced to 0.76. Despite that the large amount of heat released from the methanation reaction (i.e., 204.7 kJ/mol) will result in an expansion of the gas phase, the blowing gas is still not capable to make the particles fluidized, which indicates the dominant effect of gas-volume reduction on the fluidization quality. When the gas mass flux is raised to 0.67 kg/m^2/s, the particles could be fluidized but the fluidization quality is not good enough due to the frequent appearance of bubbles (see Fig. 1c). When the gas mass flux is raised to 1.34 kg/m^2/s, the fluidization quality is optimized with much more uniform spatial distribution of the particles (see Fig. 1d).

Table 3. Estimated superficial gas velocity and minimum fluidization velocity based on different assumptions for the gas component (Fig. 1b: G_g = 0.134 kg/m^2/s, $T_g \approx$ 1100 K)

Gas component (vol%)	ρ_g (kg/m^3)	U_g (m/s)	*Ar*	U_{mf} (m/s) (*)	U_g/U_{mf}
25 CO + 75 H_2	1.6730	0.0801	179.0	0.0497	1.61
50 CH_4 + 50 H_2O	3.3459	0.0400	358.0	0.0529	0.76

(*) calculated through the drag force formula by Di Felice (11) balanced with the gravity force.

Fig. 2 shows the variations of CO conversion and selectivity to methane with the gas flux at a fixed inlet gas temperature of 673 K. The CO conversion at the gas mass flux of 0.67 kg/m^2/s is smaller than the ones at the other two conditions, which mainly suffers from the bad fluidization quality. A part of the reacting gas moves up through the bubbles in the fluidized bed directly, undergoing worse gas-particle contact efficiency and shorter gas-particle contact time in comparison with the other two cases. When the fluidization quality is optimized, the CO conversion approaches to 100% under the conditions of good gas-particle contact efficiency, despite of the relative short gas residence time at the largest gas mass flux among the three cases.

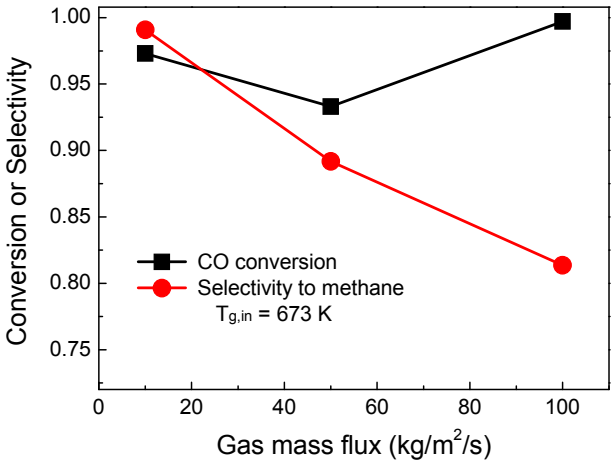

Figure 2. Variations of CO conversion and selectivity to methane with the gas mass flux ($T_{g,in}$ = 673 K; the time-averaged performances of the reactor are calculated from the transient results between 1.0 and 1.5 s for each case statistically)

It can be also found that the selectivity to methane is decreased with the increase of gas mass flux as shown in Fig. 2. One probable reason for this observation is that the steam reforming of methane to carbon dioxide is promoted by the rapidly raised reaction temperature due to the highly exothermal methanation reaction. As shown in Fig. 3a, a local hot-spot up to 1500 K could be found from the transient field of the gas temperature, which is favorable for the formation of CO_2. However, almost all of the particles remain temperature below 1000 K, which could be further controlled by strengthening the heat removal from the reactor wall. In present simulations, the gas-wall heat transfer coefficient is set at a low level of heat removal (i.e., 10 W/m^2/K) to investigate the effect of high gas temperature on the particle phase. In practice, much more reaction heat could be removed through the reactor wall and internals. At the same operating conditions and reactor geometry for another fixed-bed reactor, it is found that the particles suffer from the high temperature approximating to the high gas temperature of about 1500 K (see Fig. 3b). It should be mentioned that the particles could not stand such a high temperature as 1500 K in a real fixed-bed reactor. This result just appears in the simulations based on the assumptions that the catalyst particles could survive at a high temperature up to 1500 K and remain their catalytic activity. Further improvements are planned for current model.

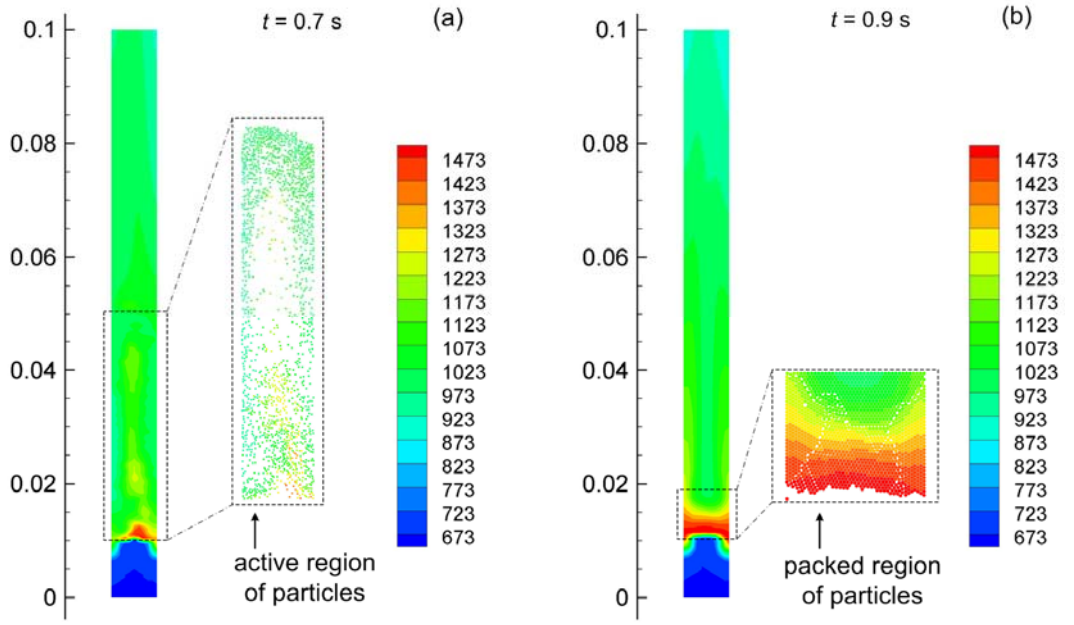

Figure 3. Transient spatial distributions of the gas and particle temperatures: (a) fluidized-bed reactor, (b) fixed-bed reactor. ($T_{g,in}$ = 673 K, G_g = 1.34 kg/m^2/s)

Influence of Inlet Gas Temperature

The variations of CO conversion and selectivity to methane with the inlet gas temperature at different gas mass fluxes are plotted in Fig. 4. At the gas mass flux of

1.34 kg/m^2/s corresponding to good fluidization quality, the CO conversion and selectivity to methane vary with the gas feeding rate monotonically. The less CO conversion with a higher gas mass flux is caused by the increasing CO formation from methane steam reforming and reverse water gas shift reaction (i.e., Eqs. (4) and (7), respectively) at a higher reaction temperature. The higher selectivity to methane is mainly caused by the shorter reaction time with less consumption of methane. While, at the gas mass flux of 0.67 kg/m^2/s corresponding to a longer reaction time, the CO conversion is found to be larger and the selectivity to methane smaller than the ones at the gas mass flux of 1.34 kg/m^2/s expect the case of $T_{g,in}$ = 673 K. The excluded case is due to the bad fluidization quality, which is not observed in other two cases. In such unwanted fluidization, more gas moves upward directly with less gas back-mixing and radial transportation in comparison with the other two cases, which leads to the lower conversion and higher selectivity to methane.

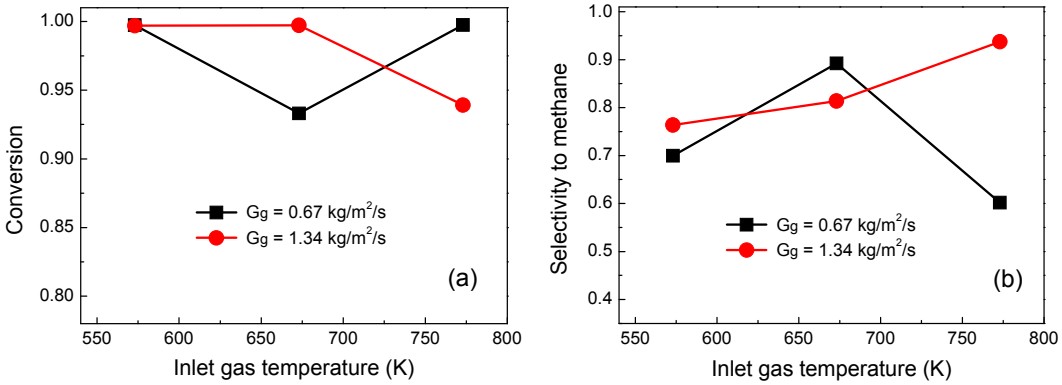

Figure 4. Variations of (a) CO conversion and (b) selectivity to methane with the inlet gas temperature at different gas mass flux

CONCLUSIONS

The CFD-DEM coupled approach was applied to simulate the complex reacting flows in fluidized-bed syngas-to-methane (STM) reactors at lab scale. Defluidization was observed under some operating conditions due to the large decrease in the numbers of moles during methanation reaction. The fluidization quality and reactor performances could be improved by optimization of the operating conditions, e.g., gas mass flux, inlet gas temperature and heat removal capacity through the wall. The fluidized-bed reactor showed good performances in heat transportation, which is favorable to prevent the catalyst particles from overheating and sintering.

ACKNOWLEDGMENT

The authors thank the financial supports from National Natural Science Foundation of China (NSFC) under the grant of No. 20806045 and PetroChina.

NOTATION

Greek letters

a_i, b_i, c_i, d_i stoichiometric coefficients, -
A_i frequency factor
Ar Archimedes number, -
E_i activation energy, J/mol
f_{cell} fractional volume of a particle residing in the cell, -
G_g gas mass flux, kg/m^2/s
p pressure, Pa
r_i reaction rate, mol/m^3/s
R gas constant, 8.314 J/mol/K
t time, s
T temperature, K
U_g superficial gas velocity, m/s
U_{mf} minimum fluidization velocity, m/s
V_{cell} volume of computational cell, m^3
V_p^i volume of particle i, m^3
ΔH_i heat of reaction i, J/mol
ε porosity, -
$\varepsilon_{p,0}$ initial solid volume fraction, -
φ general variable
ρ_g gas density, kg/m^3

Subscripts

0 initial state
g gas phase
i numerical number of particles or species
in inlet
p particle phase

REFERENCES

(1) Hirsch R.L., Gallagher J.E., Lessard R.R., Wesselhoft R.D., 1982. Catalytic coal gasification: An emerging technology. *Science* **215**, 121-126.

(2) Wender I., 1996. Reactions of synthesis gas. *Fuel Proc. Technol.* **48**, 189-297.

(3) Kai T., Furusaki S., Yamamoto K., 1984. Methanation of carbon monoxide by a fluidized catalyst bed. *J. Chem. Eng. Japan* **17**, 280-285.

(4) Kai T., Toriyama K., Nishie K., Takahashi T., Nakajima M., 2006. Effect of volume decrease on fluidization quality of fluidized catalyst beds. *A.I.Ch.E. J.* **52**, 3210-3215.

(5) Zhu J.X., Cheng Y., 2006. Fluidized-Bed Reactors and Applications, In: *Multiphase Flow Handbook*, Crowe C.T. (Ed.), CRC Press (Taylor & Francis Group): Boca Raton, pp. (5-55)~(5-83).

(6) Wu C.N., Cheng Y., Ding Y.L., Jin Y., 2010. CFD-DEM simulation of gas-solid reacting flows in fluid catalytic cracking (FCC) process. *Chem. Eng. Sci.* **65**, 542-549.

(7) Cundall, P.A., Strack, O.D.L., 1979. A discrete numerical model for granular assemblies. *Geotechnique* **29**, 47-65.

(8) Iwashita K., Oda M., 1998. Rolling resistance at contacts in simulation of shear band development by DEM. *J. Eng. Mechanics* **124**, 285-292.

(9) Vargas W., McCarthy J., 2001. Heat conduction in granular materials. *A.I.Ch.E. J.* **47**, 1052-1059.

(10) Hoomans B.P.B., Kuipers J.A.M., Briels W.J., Van Swaaij W.P.M., 1996. Discrete particle simulation of bubble and slug formation in a two-dimensional gas-fluidised bed: a hard-sphere approach. *Chem. Eng. Sci.* **51**, 99-118.

(11) Di Felice R., 1994. The voidage function for fluid-particle interaction systems. *Int. J. Multiphase Flow* **20**, 153-159.